Frontiers | Frontiers in Physics

Volumetric absorption illumination induced by laser radiation in a 2D thermoelastic microelongated semiconductor body with temperature-dependent properties

Ismail M. Tayel[1]*, Jawdat Alebraheem[1]*, Mogtaba Mohammed[1,2]*, Khaled Lotfy[3,4]* and Alaa A. El-Bary[5,6]*

[1]Department of Mathematics, College of Science Al-Zulfi, Majmaah University, Al Majmaah, Saudi Arabia, [2]Department of Mathematics, College of Science Sudan University of Science and Technology, Khartoum, Sudan, [3]Department of Mathematics, Faculty of Science, Zagazig University, Zagazig, Egypt, [4]Department of Mathematics, Faculty of Science, Taibah University, Madinah, Saudi Arabia, [5]Arab Academy for Science, Technology and Maritime Transport, Alexandria, Egypt, [6]National Committee for Mathematics, Academy of Scientific Research and Technology, Cairo, Egypt

In this paper, we construct a new model based on the coupling of thermoelasticity, plasma, and microelongation effect under volumetric absorption of laser pulse. Three different thermoelasticity theories are applied to construct the new model in a 2D thermoelastic semiconducting medium whose properties are temperature-dependent. The medium surface is exposed to laser radiation having spatial and temporal Gaussian distributions; in addition, the surface is considered traction-free. The general solutions were obtained analytically via Laplace and Fourier transformations; for Laplace inverse, we use the well-known Riemann sum approximation. As an application and consistency validation, silicon material is used.

1 Introduction

Biot is credited by developing the coupling between temperature and strain in his formulation of the classical coupled theory of thermoelasticity (CTE) in 1956 [1]. However, a flaw in this theory gave rise to the concept of generalized thermoelasticity; see, for instance, [2]. The first generalization was proposed by Lord and Shulman (LS) [3]; instead of relying on Fourier's law, LS's theory relies on another heat conduction law involving relaxation time [4, 5]. Hence, the produced thermal waves are physically accepted; see [6]. Due to its application in thermoelasticity, this theory has been widely used in many studies [7, 8]. Green and Lindsay (GL) [9] followed LS's theory with a generalization with two relaxation times that considered temperature–rate dependence. This theory has been applied in many problems of thermoelasticity, making it an essential part of its development; see [10, 11].

Semiconductor materials, which have a wide range of applications in physics and engineering, are among the most significant materials that have directly influenced technological advancement [12, 13]. Thermoelasticity (TE) and the deformation of electrons DE are the two basic mechanisms that are produced when a semiconductor surface is subjected to a laser beam; for further information, see [14]. Recently, the relationship involving TE and DE has become necessary, which increases the viability of using generalized theories to study wave propagation in a semiconductor medium [15]. Various generalizations were used by Lotfy and Lotfy et al. [16–18] to examine the photothermal illumination phenomenon in various results. Ezzat [19] used a novel model within the context of time-fractional derivatives to examine the impacts of combined plasma and thermal waves in a viscoelastic material. In semi-infinite semiconductor materials with such a cylindrical cavity exposed to thermal shock under a simulated model considering variable thermal conductivity, for the investigation of photothermoelastic consequences, we refer to [20]. Youssef and El-Bary [21] addressed a two-dimensional semiconductor material cylinder driven by ramp-type heat through the use of the LS framework to discuss photothermoelastic coupling. More recently, Tayel and Lotfy [22] and Mohammed and Tayel [23] studied the photothermal effects induced by a laser pulse under the new modification of Green and Lindsay (MGL).

Due to the numerous uses of thermoelasticity, the study of materials whose characteristics are temperature-dependent has become increasingly important. The overwhelming majority of results now available on thermoelasticity are achieved for temperature-independent material, despite the fact that components fluctuate at high temperatures; for examples, see [24, 25] and the references within. In terms of the generalized thermoelasticity, some valuable works with significant results for understanding the effect of the influences of temperature-dependent features could be seen in [26–29].

Many applications have been introduced in the fields of science and engineering based on special features of lasers. In material processing various fields such as cutting, drilling of holes, glazing of materials, and spot welding, high-power lasers are utilized [30, 31]. In semiconductor material, excitation caused by laser radiation generates three different waves: thermal, elastic, and plasma waves. Several papers have discussed the transportation processes induced by the laser pulse in semiconductor materials; see [32–36].

Microelongated materials can be found in many branches of material science; some examples of microelongated media involve solid–liquid crystals, structural materials reinforced with crushed elastic fibers, and porous materials having pores stuffed to the gills with gases or non-viscous fluid. It should be noted that numerous effects on microelongated thermoelasticity, such as initial stress, and also comparing relaxation times including their effects on all physical parameters, have not received much attention; see [37–41].

In this paper, we shall discuss the volumetric absorption of laser radiation in a 2D thermoelastic microelongated semiconducting half space whose properties are temperature-dependent. We introduce a novel model based on the coupling of TE, plasma, and microelongation waves by means of three different theories of thermoelasticity, namely, CTE, LS, and GL. Moreover, the temperature-dependent properties are investigated through all the aforementioned waves.

2 Problem setting and basic equations

In what follows, we introduce the system of governing equations that consider the microelongation effect coupled with plasma and TE response. We start by

Energy is represented as follows [38]:

$$
\kappa T_{,ii} - \rho C_E \left(n_1 + \tau_0 \frac{\partial}{\partial t} \right) \dot{T} - \gamma_1 T_0 \left(n_1 + n_0 \tau_0 \frac{\partial}{\partial t} \right) \dot{u}_{i,i} + \frac{E_g}{\tau} N - \gamma_2 T_0 \dot{\varphi}
$$
$$
= - \left(n_1 + n_0 \tau_0 \frac{\partial}{\partial t} \right) Q(x, z, t). \tag{1}
$$

The plasma wave equation, which depicts the interaction between plasma and temperature, is as follows [13]:

$$
\dot{N} = D_E N_{,ii} - \frac{N}{\tau} + \kappa T. \tag{2}
$$

The equation of motion is given as follows [18, 42]:

$$
(\lambda + \mu) u_{j,ij} + \mu u_{i,jj} + \lambda_1 \varphi_{,i} - \gamma_1 \left(1 + v_0 \frac{\partial}{\partial t} \right) T_{,i} - \delta_n N_{,i} = \rho \ddot{u}_i. \tag{3}
$$

Microelongation is represented as follows [18, 42]:

$$
\alpha \varphi_{,ii} - \lambda_2 \varphi - \lambda_1 u_{j,j} + \gamma_2 \left(1 + v_0 \frac{\partial}{\partial t} \right) T = \frac{1}{2} j \rho \ddot{\varphi}. \tag{4}
$$

The microelongation constitutive equation is as follows [43–45]:

$$
\left. \begin{array}{l}
\sigma_{ij} = (\lambda_1 \varphi + \lambda u_{r,r}) \delta_{ij} + 2\mu u_{j,i} - \gamma_1 \left(1 + v_0 \frac{\partial}{\partial t} \right) T \delta_{ij} - ((3\lambda + 2\mu) d_n N) \delta_{ij}, \\[2mm]
m_i = a_0 \varphi_{,i}, \\[2mm]
s - \sigma = \lambda u_{i,i} - \gamma_2 \left(1 + v_0 \frac{\partial}{\partial t} \right) T + -((3\lambda + 2\mu) d_n N) \delta_{2i} + \lambda_1 \varphi.
\end{array} \right\} \tag{5}
$$

where $\kappa = \frac{1}{\tau} \frac{\partial n_0}{\partial T}$, $\gamma_1 = (3\lambda + 2\mu)\alpha_{t1}$, $\delta_n = (3\lambda + 2\mu) d_n$, and $\gamma_2 = (3\lambda + 2\mu)\alpha_{t2}$. For a volumetric technique of heating, we let

$$
Q(x, z, t) = A_0 q_0 \xi e^{-\xi x} Q(z, t).
$$

The aforementioned system of equations can be classified according to the values of n_0 and n_1 as follows:

1. The classical coupled theory of thermoelasticity (CTE), when $n_1 = 1$, $n_0 = 0$, $\tau_0 =$, and $v_0 = 0$.
2. Lord and Shulman theory (LS) when $n_1 = n_0 = 1$, $v_0 = 0$, and $\tau_0 > 0$.
3. Green and Lindsay theory (GL), when $n_1 = 1$, $n_0 = 0$, and $v_0 > \tau_0 > 0$.

Consider a TE isotropic and homogeneous microelongated semiconducting 2D half space to be at a reference temperature T_0. The medium surface $x = 0$ is subjected to a laser pulse and considered traction-free.

Due to the two-dimensional effect of ED and TE deformations, we assume that our primary fields depend on (x, z, t). In this setting,

the scalar microelongational function in the *xz*-plane and displacement tensor u_i will be written as follows:

$$\left.\begin{array}{l} \varphi = \varphi(x, z, t) \\ \vec{u} = (u, 0, w), \quad u = u(x, z, t), \quad w = w(x, z, t) \end{array}\right\}. \qquad (6)$$

Thus, the cubic dilatation is expressed as follows:

$$e = \frac{\partial u}{\partial x} + \frac{\partial w}{\partial z}. \qquad (7)$$

Let us assume the following parameters to be temperature-dependent; see [28, 46]:

$$\begin{array}{l} \{k, \gamma_1, E_g, \gamma_2, D_E, \kappa, \lambda, \mu, \lambda_1, \lambda_2, \delta n, \alpha\} \\ = \{k_0, \gamma_{1_0}, E_{g0}, \gamma_{2_0}, D_{E0}, \kappa_0, \lambda_0, \mu_0, \lambda_{1_0}, \lambda_{2_0}, \delta n_0, \alpha_0\} f(T_0), \end{array} \qquad (8)$$

where $f(T_0)$, a given linear dimensionless function, takes the form

$$f(T_0) = 1 - \zeta f(T_0), \qquad (9)$$

and ζ is an empirical parameter.

Consequently, our system becomes (2)–(1):

$$k_0 \nabla^2 \theta - \frac{\rho C_E}{f(T_0)} \left(n_1 + \tau_0 \frac{\partial}{\partial t} \right) \frac{\partial \theta}{\partial t} - \gamma_{1_0} T_0 \left(n_1 + n_0 \tau_0 \frac{\partial}{\partial t} \right) \frac{\partial e}{\partial t} + \frac{E_{g_0}}{\tau} N$$
$$- \gamma_{2_0} T_0 \dot{\varphi} = -\frac{1}{f(T_0)} A_0 q_0 \xi \left(n_1 + n_0 \tau_0 \frac{\partial}{\partial t} \right) e^{-\xi x} Q(z, t), \qquad (10)$$

$$D_{E_0} \nabla^2 N - \frac{N}{f(T_0)\tau} + \kappa_0 \theta = \frac{1}{f(T_0)} \frac{\partial N}{\partial t}, \qquad (11)$$

$$\alpha_0 \nabla^2 \varphi - \lambda_{2_0} \varphi - \lambda_{1_0} e + \gamma_{2_0} \left(1 + v_0 \frac{\partial}{\partial t} \right) \theta = \frac{1}{2 f(T_0)} j \rho \ddot{\varphi}, \qquad (12)$$

$$(\lambda_0 + \mu_0) \frac{\partial e}{\partial x} + \mu_0 \nabla^2 u + \lambda_{1_0} \frac{\partial \varphi}{\partial x} - \gamma_{1_0} \left(1 + v_0 \frac{\partial}{\partial t} \right) \frac{\partial \theta}{\partial x} - \delta_{n_0} \frac{\partial N}{\partial x}$$
$$= \frac{\rho}{f(T_0)} \frac{\partial^2 u}{\partial t^2}, \qquad (13)$$

and

$$(\lambda_0 + \mu_0) \frac{\partial e}{\partial z} + \mu_0 \nabla^0 w + \lambda_{1_0} \frac{\partial \varphi}{\partial z} - \gamma_{1_0} \left(1 + v_0 \frac{\partial}{\partial t} \right) \frac{\partial \theta}{\partial z} - \delta_{n_0} \frac{\partial N}{\partial z}$$
$$= \frac{\rho}{f(T_0)} \frac{\partial^2 w}{\partial t^2}. \qquad (14)$$

$$\left.\begin{array}{l} \sigma_{xx} = f(T_0) \left(2\mu_0 \frac{\partial u}{\partial x} + \lambda_0 e - \gamma_{1_0} \left(1 + v \frac{\partial}{\partial t} \right) T - \delta_{n_0} N + \lambda_{1_0} \varphi \right), \\[2mm] \sigma_{zz} = f(T_0) \left(2\mu_0 \frac{\partial w}{\partial z} + \lambda_0 e - \gamma_{1_0} \left(1 + v \frac{\partial}{\partial t} \right) T - \delta_{n_0} N + \lambda_{1_0} \varphi \right), \\[2mm] \sigma_{yy} = f(T_0) \left(\lambda_0 e - \gamma_{1_0} \left(1 + v \frac{\partial}{\partial t} \right) T - \delta_{n_0} N + \lambda_{1_0} \varphi \right), \\[2mm] \sigma_{xz} = \mu_0 f(T_0) \left(\frac{\partial u}{\partial z} + \frac{\partial w}{\partial x} \right). \end{array}\right\}, \qquad (15)$$

where $\theta = T - T_0$ is the increment of the temperature.

We now introduce the initial and boundary conditions for the considered problem as follows: The initial conditions are

$$\left.\begin{array}{l} \theta = \dfrac{\partial \theta}{\partial t} = 0, \\[3mm] N = \dfrac{\partial N}{\partial t} = 0, \\[3mm] \{u, w\} = \dfrac{\partial \{u, w\}}{\partial t}, \\[3mm] \phi = \dfrac{\partial \phi}{\partial t} = 0, \end{array}\right\} \qquad (16)$$

and the boundary conditions become

$$\left.\begin{array}{l} \dfrac{\partial \theta}{\partial x}(0, z, t) = 0, \\[3mm] D_E \dfrac{\partial N}{\partial x}(0, z, t) = s_0 N(0, z, t), \\[3mm] \sigma_{xx}(0, z, t) = \sigma_{xz}(0, z, t) = 0, \\[3mm] \phi(0, z, t) = 0, \end{array}\right\} \qquad (17)$$

where s_0 is the surface recombination velocity. It is possible to use dimensionless variables to make the computations simpler, such as

$$\left.\begin{array}{l} \tilde{N} = \dfrac{\delta_n}{T_0 \gamma_{1_0}} N, \quad \tilde{x}_i = \dfrac{\omega^\star}{C_1} x_i, \quad \tilde{u}_i = \dfrac{\rho C_1 \omega^\star}{T_0 \gamma_{1_0}} u_i, \quad (\tilde{t}, \tilde{\tau}_0, \tilde{v}_0) = \omega^\star(t, \tau_0, v_0), \\[3mm] C_1^2 = \dfrac{2\mu + \lambda}{\rho}, \quad \tilde{\theta} = \dfrac{\theta}{T_0}, \quad \tilde{\sigma}_{ij} = \dfrac{\sigma_{ij}}{T_0 \gamma_{1_0}}, \quad \tilde{\varphi} = \dfrac{\rho C_1^2}{T_0 \gamma_{1_0}} \varphi, \quad \omega^\star = \dfrac{\rho C_E C_1^2}{K}, \quad C_2^2 = \dfrac{\mu}{\rho}, \end{array}\right\}. \qquad (18)$$

In computations, the primary governing equations are simplified using Eq. 18, which results in the following:

$$\nabla^2 \theta - \epsilon_1 \left(n_1 + \tau_0 \frac{\partial}{\partial t} \right) \frac{\partial \theta}{\partial t} - \epsilon_2 \left(n_1 + n_0 \tau_0 \frac{\partial}{\partial t} \right) \frac{\partial e}{\partial t} + \epsilon_3 N - \epsilon_4 \dot{\varphi}$$
$$= -\epsilon_1 A_0 q_0 \xi \left(n_1 + n_0 \tau_0 \frac{\partial}{\partial t} \right) e^{-\xi x} Q(z, t), \qquad (19)$$

$$\left(\nabla^2 - \epsilon_5 - \epsilon_6 \frac{\partial}{\partial t} \right) N + \epsilon_7 \theta = 0, \qquad (20)$$

$$\nabla^2 \varphi - C_3 \varphi - C_5 e + C_6 \left(1 + v_0 \frac{\partial}{\partial t} \right) \theta - C_4 \ddot{\varphi} = 0, \qquad (21)$$

$$\left(\frac{\lambda + \mu}{\rho C^2} \right) \frac{\partial e}{\partial x} + \frac{\mu}{\rho c^2} \nabla^2 u + \frac{\lambda_{1_0}}{\rho c^2} \frac{\partial \varphi}{\partial x} - \left(1 + v_0 \frac{\partial}{\partial t} \right) \frac{\partial \theta}{\partial x} - \frac{\partial N}{\partial x}$$
$$= \frac{1}{f(T_0)} \frac{\partial^2 u}{\partial t^2}, \qquad (22)$$

and

$$\left(\frac{\lambda + \mu}{\rho C^2} \right) \frac{\partial e}{\partial z} + \frac{\mu}{\rho c^2} \nabla^2 w + \frac{\lambda_{1_0}}{\rho c^2} \frac{\partial \varphi}{\partial z} - \left(1 + v_0 \frac{\partial}{\partial t} \right) \frac{\partial \theta}{\partial z} - \frac{\partial N}{\partial z}$$
$$= \frac{1}{f(T_0)} \frac{\partial^2 w}{\partial t^2}. \qquad (23)$$

The constitutive relations according to Eq. 5 can be written as follows:

$$\sigma_{xx} = f(T_0) \left[a_2 \frac{\partial u}{\partial x} + a_3 e - \left(1 + v_0 \frac{\partial}{\partial t} \right) \theta - N + a_1 \varphi \right], \qquad (24)$$

$$\sigma_{zz} = f(T_0) \left[a_2 \frac{\partial w}{\partial z} + a_3 e - \left(1 + v_0 \frac{\partial}{\partial t} \right) \theta - N + a_1 \varphi \right], \qquad (25)$$

$$\sigma_{yy} = f(T_0) \left[a_3 e - \left(1 + v_0 \frac{\partial}{\partial t} \right) \theta - N + a_1 \varphi \right], \qquad (26)$$

$$\sigma_{xz} = a_4 f(T_0)\left(\frac{\partial u}{\partial z} + \frac{\partial w}{\partial x}\right), \qquad (27)$$

and the boundary conditions become

$$\left.\begin{array}{l} \dfrac{\partial \theta}{\partial x}(0, z, t) = 0, \\[2mm] \dfrac{\partial N}{\partial x}(0, z, t) = \epsilon_8 N(0, z, t), \\[2mm] \sigma_{xx}(0, z, t) = \sigma_{xz}(0, z, t) = 0, \\[2mm] \phi(0, z, t) = 0. \end{array}\right\}. \qquad (28)$$

Here, we combine Eqs. 22, 23 to become

$$\nabla^2 e + a_1 \nabla^2 \varphi - \left(1 + \nu_0 \frac{\partial}{\partial t}\right)\nabla^2 \theta - \nabla^2 N = \epsilon_1 \frac{\partial^2 e}{\partial t^2}, \qquad (29)$$

where

$$\epsilon_1 = \frac{1}{f(T_0)}, \quad \epsilon_2 = \frac{T_0 \gamma_{1_0}^2}{\rho k_0 \omega}, \quad \epsilon_3 = \frac{E_{g_0} \gamma_{1_0} C_1^2}{\tau \delta_{n_0} k_0 \omega}, \quad \epsilon_4 = \frac{T_0 \gamma_{1_0} \gamma_{2_0}}{\rho k_0 \omega}$$

$$\epsilon_5 = \frac{C_1^2}{\tau D_{E_0} \omega f(T_0)}, \quad \epsilon_6 = \frac{C_1^2}{D_{E_0} \omega f(T_0)}, \quad \epsilon_7 = \frac{k_0 C_1^2 \delta_{n_0}}{\tau D_{E_0} \gamma_{1_0} \omega},$$

$$\epsilon_8 = \frac{s_0 C_1}{D_{E_0} w f(T_0)},$$

$$C_3 = \frac{\lambda_{20} C_1^2}{\alpha_0 \omega^2}, \quad C_4 = \frac{\rho J C_1^2}{2 f(T_0) \alpha_0}, \quad C_5 = \frac{\lambda_{10} C_1^2}{\alpha_0 \omega^2}, \quad C_6 = \frac{\gamma_{20} \rho C^4}{\alpha_0 \gamma_{10} \omega^2}$$

$$a_1 = \frac{\lambda_{10}}{\rho C_1^2}, \quad a_2 = \frac{2\mu_0}{\rho C_1^2}, \quad a_3 = \frac{\lambda_0}{\rho C_1^2}, \quad a_4 = \frac{a_2}{2}.$$

3 Problem solution

The method of integral transformation will be applied using the first Laplace transform for the variable of t and then the Fourier transform for the coordinate z.Now, introduce Laplace transform

$$\bar{f}(x, z, s) = \int_0^\infty f(x, z, t) e^{-st} dt. \qquad (30)$$

Then, Fourier transform

$$\hat{\bar{f}}(x, p, s) = \frac{1}{\sqrt{2\pi}} \int_{-\infty}^\infty \bar{f}(x, z, s) e^{-ipz} dz. \qquad (31)$$

Applying Fourier and Laplace transformations for Eqs. 19–21 and Eq. 22, this gives the following system:

$$(D^2 - p^2 - \beta_1)\hat{\bar{\theta}} - \beta_2 \hat{\bar{e}} + \epsilon_3 \hat{\bar{N}} - \epsilon_4 s\hat{\bar{\varphi}} = -A_0 q_0 \xi \beta_7 e^{-\xi x} \hat{\bar{Q}}(p, s), \quad (32)$$

$$(D^2 - p^2 - \beta_3)\hat{\bar{N}} + \epsilon_7 \hat{\bar{\theta}} = 0, \qquad (33)$$

$$(D^2 - p^2 - \beta_4)\hat{\bar{\varphi}} - C_5 \hat{\bar{e}} + \beta_5 \hat{\bar{\theta}} = 0, \qquad (34)$$

$$(D^2 - p^2 - \epsilon_1 s^2)\hat{\bar{e}} + a_1(D^2 - p^2)\hat{\bar{\varphi}} - \beta_6(D^2 - p^2)\hat{\bar{\theta}} \qquad (35)$$
$$- (D^2 - p^2)\hat{\bar{N}} = 0,$$

where $\hat{\bar{Q}}(p, s)$ is $Q(z, t)$ in the transformed domain, and

$$\beta_1 = \epsilon_1 s(n_1 + s\tau_0), \ \beta_2 = \epsilon_2 s(n_1 + n_0 s\tau_0), \ \beta_3 = \epsilon_5 + \epsilon_6 s,$$
$$\beta_4 = C_3 + C_4 s^2, \beta_5 = C_6(1 + \nu_0 s), \beta_6 = (1 + \nu_0 s), \beta_7 = \epsilon_1(n_1 + s\tau_0).$$

Eliminating $\hat{\bar{\theta}}$ and $\hat{\bar{e}}$ from Eqs. 32–35, we obtain the following:

$$[c_5((D^2 - p^2 - \beta_1)(D^2 - p^2 - \beta_3) - \epsilon_3 \epsilon_7) - \beta_2 \beta_5(D^2 - p^2 - \beta_3)]\hat{\bar{N}}$$
$$+ (\beta_2 \epsilon_7(D^2 - p^2 - \beta_4) + \epsilon_4 \epsilon_7 c_5 s)\hat{\bar{\varphi}} = A_0 q_0 c_5 \epsilon_7 \beta_7 \xi e^{-\xi x} \hat{\bar{Q}}(p, s), \qquad (36)$$

and

$$\epsilon_7[(D^2 - p^2 - \epsilon_1 s^2)(D^2 - p^2 - \beta_4) + a_1 c_5(D^2 - p^2)]\hat{\bar{\varphi}}$$
$$+ [(D^2 - p^2 - \beta_3)(-\beta_5(D^2 - p^2 - \epsilon_1 s^2) + c_5 \beta_6(D^2 - p^2)) \quad (37)$$
$$- \epsilon_7 c_5(D^2 - p^2)]\hat{\bar{N}} = 0.$$

Eliminating $\hat{\bar{\varphi}}$ from (36) and (37), we get

$$(D^8 - b_1 D^6 + b_2 D^4 - b_3 D^2 + b_4)\hat{\bar{N}} = G_1 e^{-\xi x}, \qquad (38)$$

where

$$G_1 = A_0 q_0 \beta_7 \epsilon_7 \left[(\xi^2 - p^2 - \epsilon_1 s^2)(\xi^2 - p^2 - \beta_4)\right.$$
$$\left. + a_1 c_5(\xi^2 - p^2)\right]\xi \hat{\bar{Q}}(p, s)$$

and

$$b_1 = -(-4p^2 + a_1 C_5 - \beta_1 - \beta_3 - \beta_4 - \beta_2 \beta_6 - s^2 \epsilon_1),$$

$$b_2 = 6p^4 + 3\beta_3 p^2 + 3\beta_4 p^2 + 3\beta_2 \beta_6 p^2 + 3s^2 \epsilon_1 p^2 + \beta_3 \beta_4 - sC_5 \beta_6 \epsilon_4$$
$$- a_1(C_5(3p^2 + \beta_1 + \beta_3) + \beta_2 \beta_5) + \beta_2 \beta_3 \beta_6 + \beta_2 \beta_4 \beta_6 + \beta_2 \epsilon_7$$
$$+ s^2 \beta_3 \epsilon_1 + s^2 \beta_4 \epsilon_1 + \beta_1(3p^2 + \beta_3 + \beta_4 + s^2 \epsilon_1) + s\beta_5 \epsilon_4 - \epsilon_3 \epsilon_7,$$

$$b_3 = -4p^6 - 3\beta_3 p^4 - 3\beta_4 p^4 - 3\beta_2 \beta_6 p^4 - 3s^2 \epsilon_1 p^4 - 2\beta_3 \beta_4 p^2 - 2\beta_2 \beta_3 \beta_6 p^2$$
$$- 2\beta_2 \beta_4 \beta_6 p^2 - 2s^2 \beta_3 \epsilon_1 p^2 - 2s^2 \beta_4 \epsilon_1 p^2 - 2s\beta_5 \epsilon_4 p^2 + 2sC_5 \beta_6 \epsilon_4 p^2$$
$$- 2\beta_2 \epsilon_7 p^2 + 2\epsilon_3 \epsilon_7 p^2 - \beta_2 \beta_3 \beta_4 \beta_6 - s^2 \beta_3 \beta_4 \epsilon_1 + \beta_4 \epsilon_3 \epsilon_7 - \beta_2 \beta_4 \epsilon_7$$
$$- \beta_1(3p^4 + 2s^2 \epsilon_1 p^2 + \beta_4(2p^2 + s^2 \epsilon_1) + \beta_3(2p^2 + \beta_4 + s^2 \epsilon_1))$$
$$+ s^2 \epsilon_1 \epsilon_3 \epsilon_7 + sC_5 \epsilon_4 \epsilon_7 - s\beta_3 \beta_5 \epsilon_4 + sC_5 \beta_3 \beta_6 \epsilon_4 - s^3 \beta_5 \epsilon_1 \epsilon_4$$
$$+ a_1(\beta_2(2p^2 + \beta_3)\beta_5 + C_5(3p^4 + 2\beta_3 p^2 + \beta_1(2p^2 + \beta_3) - \epsilon_3 \epsilon_7)),$$

$$b_4 = p^8 + \beta_3 p^6 + \beta_4 p^6 + \beta_2 \beta_6 p^6 + s^2 \epsilon_1 p^6 + \beta_3 \beta_4 p^4 + \beta_2 \beta_3 \beta_6 p^4$$
$$+ s^2 \beta_3 \epsilon_1 p^4 + s^2 \beta_4 \epsilon_1 p^4 + s\beta_5 \epsilon_4 p^4 - sC_5 \beta_6 \epsilon_4 p^4 + \beta_2 \epsilon_7 p^4 - \epsilon_3 \epsilon_7 p^4$$
$$+ \beta_2 \beta_3 \beta_4 \beta_6 p^2 + s^2 \beta_3 \beta_4 \epsilon_1 p^2 + s\beta_3 \beta_5 \epsilon_4 p^2 - sC_5 \beta_3 \beta_6 \epsilon_4 p^2 + s^3 \beta_5 \epsilon_1 \epsilon_4 p^2$$
$$+ \beta_2 \beta_4 \beta_6 p^4 - s^2 \epsilon_1 \epsilon_3 \epsilon_7 p^2 - sC_5 \epsilon_4 \epsilon_7 p^2 + \beta_2 \epsilon_7 p^2 - \beta_4 \epsilon_3 \epsilon_7 p^2$$
$$+ \beta_1(p^2 + \beta_3)(p^2 + \beta_4)(p^2 + s^2 \epsilon_1) + s^3 \beta_3 \beta_5 \epsilon_1 \epsilon_4 - s^2 \beta_4 \epsilon_1 \epsilon_3 \epsilon_7$$
$$- a_1(\beta_2(p^2 + \beta_3)\beta_5 + C_5(p^4 + \beta_3 p^2 + \beta_1(p^2 + \beta_3) - \epsilon_3 \epsilon_7))p^2.$$

Factoring Eq. 38, we obtain

$$(D^2 - k_i^2)\hat{\bar{N}} = G_1 e^{-\xi x}, \qquad (39)$$

where k_i^2 $(i = 1, \ldots, 4)$ are the roots of the characteristic equation. Eq. 39 has the following solution:

$$\hat{\bar{N}}(x) = \sum_{i=1}^4 B_i(p, s) e^{-k_i x} + H_1(\xi, s) e^{-\xi x}, \qquad (40)$$

where

$$H_1 = \frac{G_1}{\xi^2 - k_i^2}.$$

The solution in terms of $\hat{\bar{\varphi}}$ is obtained in a similar manner; we have

$$(D^8 - b_1 D^6 + b_2 D^4 - b_3 D^2 + b_4)\hat{\bar{\varphi}} = G_2 e^{-\xi x}, \qquad (41)$$

where

$$G_2 = -A_0 q_0 \beta_7 \epsilon_7 \left[(\xi^2 - p^2 - \beta_3)(-\beta_5(\xi^2 - p^2 - \epsilon_1 s^2) + c_5 \beta_6(\xi^2 - p^2))\right.$$
$$\left. - \epsilon_7 c_5(\xi^2 - p^2)\right]\xi e^{-\xi x} \hat{\bar{Q}}(p, s).$$

Eq. 41 is solved as follows:

$$\hat{\bar{\varphi}}(x) = \sum_{i=1}^4 \psi_i B_i(p, s) e^{-k_i x} + H_2 e^{-\xi x}, \qquad (42)$$

where

$$H_2 = \frac{G_2}{\xi^2 - k_i^2}, \quad (i = 1, \ldots, 4),$$

where

$$\psi_i = -\frac{\left[(k_i^2 - p^2 - \beta_3)(-\beta_5(k_i^2 - p^2 - \epsilon_1 s^2) + c_5\beta_6(k_i^2 - p^2)) - \epsilon_7 c_5(k_i^2 - p^2)\right]}{\epsilon_7\left[(k_i^2 - p^2 - \epsilon_1 s^2)(k_i^2 - p^2 - \beta_4) + a_1 c_5(k_i^2 - p^2)\right]}. \tag{43}$$

Using Eq. 33, we have

$$\widehat{\bar{\theta}}(x) = \sum_{i=1}^{4} \Gamma_i B_i (p, s) e^{-k_i x} + H_3 e^{-\xi x}, \tag{44}$$

where

$$\Gamma_i = -\frac{(k_i^2 - p^2 - \beta_3)}{\epsilon_7} \text{ and } H_3 = -\frac{(\xi^2 - p^2 - \beta_3)}{\epsilon_7} H_1. \tag{45}$$

In a similar way, we get

$$\widehat{\bar{e}}(x) = \sum_{i=1}^{4} \Lambda_i B_i (p, s) e^{-k_i x} + H_4 e^{-\xi x}, \tag{46}$$

where

$$\Lambda_i = \frac{1}{C_5 \epsilon_7} \left[\epsilon_7(k_i^2 - p^2 - \beta_4)\psi_i - \beta_5(k_i^2 - p^2 - \beta_3) \right] \tag{47}$$

and

$$H_4 = \frac{1}{C_5 \epsilon_7} \left(\epsilon_7(\xi^2 - p^2 - \beta_4)H_2 - \beta_5(\xi^2 - p^2 - \beta_3)H_1 \right). \tag{48}$$

As for the displacement, Eq. 22 can be written as follows:

$$\nabla^2 u + a_5 \frac{\partial e}{\partial x} + a_1 \frac{\partial \phi}{\partial x} - a_6 \left(1 + v_0 \frac{\partial}{\partial t}\right) \frac{\partial \theta}{\partial x} - a_6 \frac{\partial N}{\partial x} = a_7 \frac{\partial^2 u}{\partial t^2}, \tag{49}$$

where $a_5 = \frac{\lambda_0 + \mu_0}{\mu_0}$, $a_6 = \frac{\rho C_1^2}{\mu_0}$, and $a_7 = a_6 \epsilon_1$.

Using Laplace and Fourier transformation to the last equation, one gets

$$(D^2 - p^2 - a_7 s^2)\widehat{\bar{u}} = -a_5 \frac{\partial \widehat{\bar{e}}}{\partial x} - a_1 \frac{\partial \widehat{\bar{\phi}}}{\partial x} + a_6 (1 + v_0 s)\frac{\partial \widehat{\bar{\theta}}}{\partial x} + a_6 \frac{\partial \widehat{\bar{N}}}{\partial x}. \tag{50}$$

The solution of the non-homogeneous ordinary differential Eq. 50 gives

$$\widehat{\bar{u}} = -\sum_{i=1}^{4} \frac{k_i \Omega_i B_i e^{-k_i x}}{(k_i^2 - p^2 - a_7 s^2)} - \frac{\xi J e^{-\xi x}}{(\xi^2 - p^2 - a_7 s^2)} + R e^{-qx}, \tag{51}$$

where

$$\Omega_i = (-a_5 \Lambda_i - a_1 \psi_i + a_6 (1 + v_0 s)\Gamma_i + a_6),$$
$$J = (-a_5 H_4 - a_1 H_2 + a_6 (1 + v_0 s)H_3 + H_1),$$

and

$$q = \sqrt{p^2 - a_7 s^2}.$$

To get the other components, namely, $\widehat{\bar{w}}$, we will use Eq. 7 in the transformed domain; we have

$$\widehat{\bar{w}} = \frac{1}{ip} \left[\sum_{i=1}^{4} \left(\Lambda_i - \frac{k_i^2 \Omega_i}{(k_i^2 - P^2 - a_7 s^2)} \right) B_i e^{-k_i x} \right.$$
$$\left. + \left(H_4 - \frac{\xi^2 J}{(\xi^2 - P^2 - a_7 s^2)} \right) e^{-\xi x} + R q e^{-qx} \right]. \tag{52}$$

Here, we consider the stresses related to the boundary conditions only, so we have

$$\widehat{\bar{\sigma}}_{xx} = f(T_0)\left[\sigma_{1i}B_i e^{-k_i x} + \sigma_1^\star e^{-\xi x} - qR e^{-qx}\right], \tag{53}$$

$$\widehat{\bar{\sigma}}_{xz} = \frac{a_4 f(T_0)}{ip}\left[\sigma_{2i}B_i e^{-k_i x} + \sigma_2^\star e^{-\xi x} - q^\star R e^{-qx}\right], \tag{54}$$

where

$$\sigma_{1i} = a_2\left(\frac{k_i^2 \Omega_i}{k_i^2 - p^2 - a_7 s^2}\right) + a_3 \Lambda_i - (1 + v_0 s)\Gamma_i + a_1 \psi_i - 1, \tag{55}$$

$$\sigma_1^\star = a_2\left(\frac{\xi^2 J}{\xi^2 - P^2 - a_7 s^2}\right) + a_3 H_4 - (1 + v_0 s)H_3 + a_1 H_2 - H_1, \tag{56}$$

$$\sigma_{2i} = -k_i\left(\Lambda_i - \frac{k_i^2 + p^2}{k_i^2 - p^2 - a_7 s^2}\right), \tag{57}$$

$$\sigma_2^\star = -\xi\left(H_4 - \frac{\xi^2 + p^2}{\xi^2 - p^2 - a_7 s^2}\right), \tag{58}$$

and

$$q^\star = -(2p^2 + a_7 s^2). \tag{59}$$

Now, to attain the constants B_i, $(i = 1, \ldots, 4)$ and R, we use (28) to obtain the following system:

$$\left.\begin{aligned}
k_i \Gamma_i B_i &= -\xi H_3, \\
(k_i + \epsilon_8)B_i &= -(\xi + \epsilon_8)H_1, \\
\sigma_{i1}B_i - qR &= -\sigma_1^\star, \\
\sigma_{i2}B_i - q^\star R &= -\sigma_2^\star, \\
\psi_i B_i &= H_2
\end{aligned}\right\}. \tag{60}$$

From this, we complete the solution.

4 Inverse of the transformation

In this section, we obtain the inverse of the solutions derived in the aforementioned section; we start by applying the inverse Fourier transform using the following formula:

$$\bar{f}(x, z, s) = \frac{1}{\sqrt{2\pi}}\int_{-\infty}^{\infty} \widehat{\bar{f}}(x, p, s)e^{ipz}dp, \tag{61}$$

where $\bar{f}(x, z, s)$ is understood in the sense of Laplace transform. After that, an inverse by means of Laplace is needed; for this, we use the well-known Riemann sum approximation:

$$f(x, z, t) = \frac{e^{\phi t}}{t}\left[\frac{1}{2}\bar{f}(x, z, \phi) + Re\sum_{n=1}^{K}(-1)^n \bar{f}\left(x, z, \phi + \frac{in\pi}{t}\right)\right]. \tag{62}$$

For a faster convergence, we let $\phi = 4.7/t$; see [47].

5 Special case

In order to increase the visibility of our results, we shall consider a special case when obtaining the numerical results. In particular, we neglect the effect of microelongation, i.e., we take $\lambda_{1_0} = \lambda_{2_0} = \gamma_{2_0} = 0$.
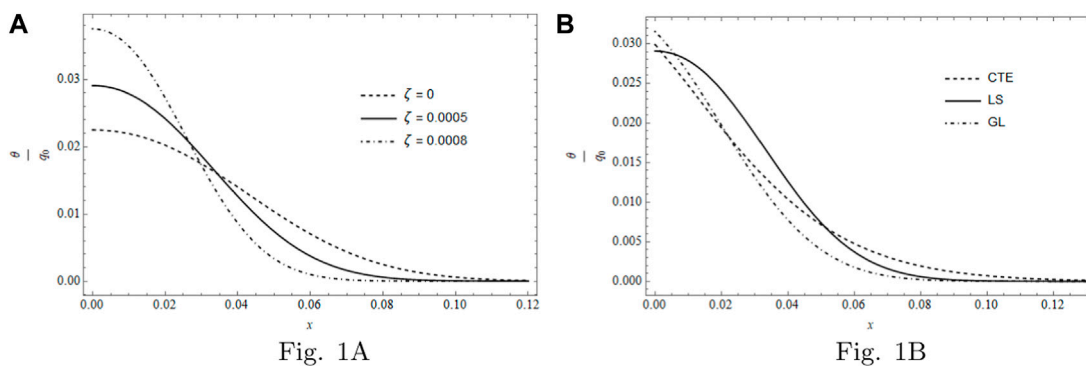
FIGURE 1
Spatial temperature distribution per q_0 at $t = 4 \times 10^{-3}$ for the aforementioned two cases.
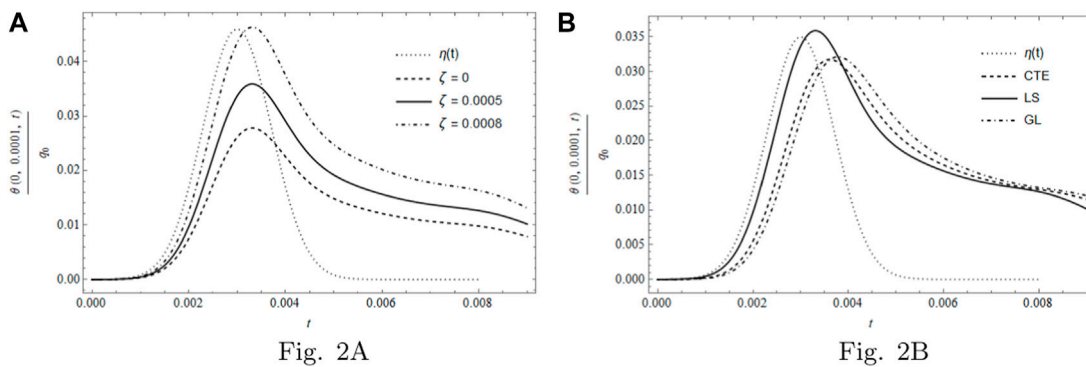
FIGURE 2
Temporal surface temperature $\theta(0, 0.0001, t)$ per q_0 for the aforementioned two cases.
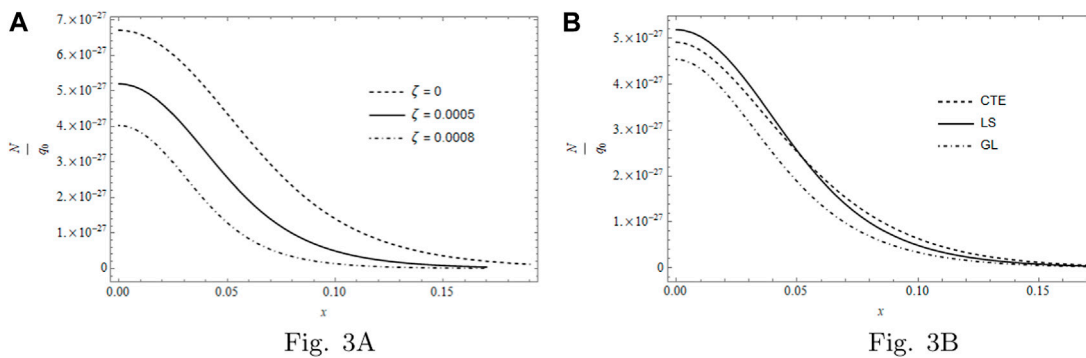
FIGURE 3
Carrier density $N(x, 1 \times 10^{-4}, 4 \times 10^{-3})$ for the aforementioned two cases.
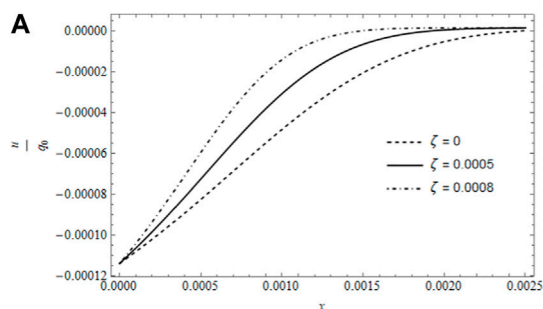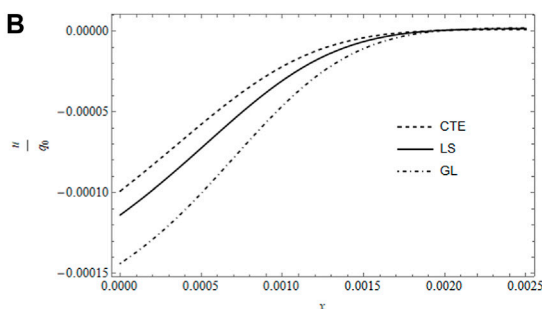
FIGURE 4
Displacement distribution $u(x, 0.0001, t)$ per q_0 for the aforementioned two cases.
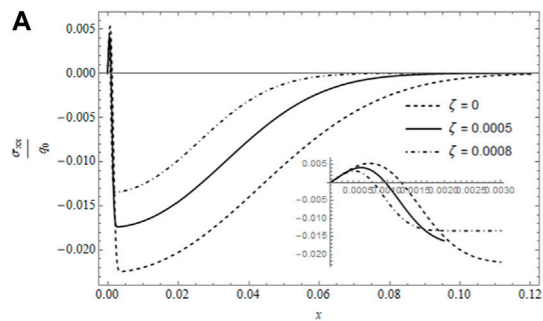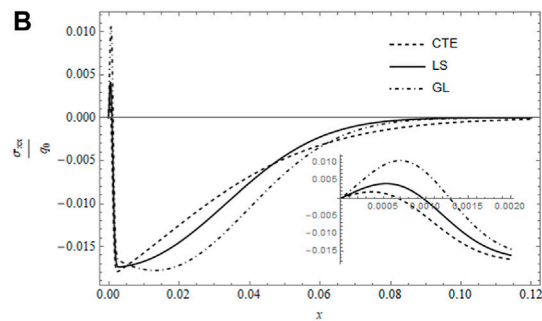
FIGURE 5
Stress σ_{xx} per q_0 for the aforementioned two cases.
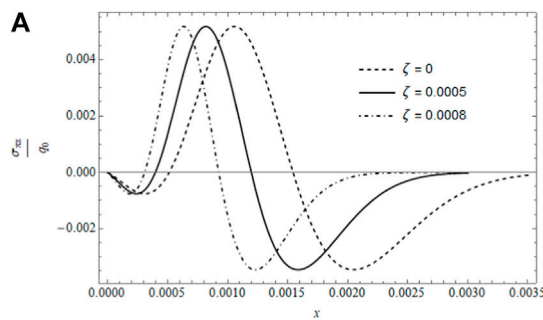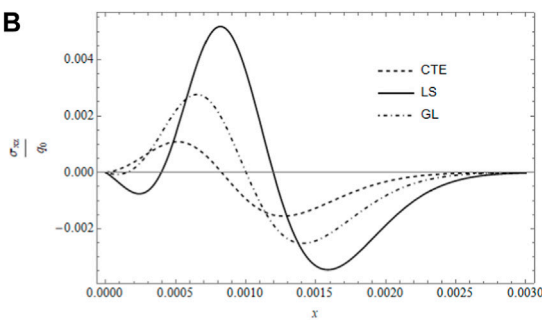
FIGURE 6
Stress σ_{xz} per q_0 for the aforementioned two cases.

6 Application

Consider a silicon material's half-space being subjected to a laser beam with a Gaussian profile as

$$Q(z, t) = V(z).\eta(t), \tag{63}$$

where $V(z) = e^{-\frac{z^2}{a^2}}$ and $\eta(t) = e^{-(\frac{t-b}{d})^2}$.

The following constants, which are based on [48], will be used to calculate the surface temperature $\theta(0, t)$, temperature θ, carrier density N displacement u, and stresses σ_{xx} and σ_{xz}.

$\alpha_{t1} = 2.59 \times 10^{-6} K^{-1}$	$k = 156 W/(m \times K)$	$T_0 = 800 K$
$\lambda = 3.64 \times 10^{10} N/m^2$	$\rho = 2330 kg/m^3$	$\tau_1 = 0.001$
$\mu = 5.46 \times 10^{10} N/m^2$	$E_{g_0} = 1.11 eV$	$\tau = 10^{-5} s$
$C_E = 695 J/(kg \times K)$	$n_0 = 10^{20} m^{-3}$	$\delta_0 = 2 m/s$
$D_E = 2.5 \times 10^{-3} m^2/s$	$a = 3 \times 10^{-3} s$	$A_0 = 0.69$
$\alpha_{1_0} = -9 \times 10^{-31} m^3$	$\tau_0 = 0.00075$	$b = 10^{-3} s.$

7 Numerical investigation

The computational results are divided into two groups. Group A shows the effect of the temperature-dependent properties for LS theory, while group B describes the consistency of the results through three different models. Through this, all the calculations are carried out for $t = 4 \times 10^{-3}$ and $z = 0.0001$.

Figure 1 is combined of two sub-graphs. Figure 1A represents θ/q_0 at $t = 4 \times 10^{-3}$ for different ζ values, namely, $\zeta = 0$, $\zeta = 5 \times 10^{-4}$ and $\zeta = 8 \times 10^{-4}$ for LS theory. Figure 1B depicts θ/q_0 at $t = 4 \times 10^{-3}$ for a fixed ζ value, that is, $\zeta = 5 \times 10^{-4}$ by taking into account three different models: LS, CTE, and GL. From the two sub-figures, we note that the temperature reached its maximum at the irradiated surface and then declined inside the medium until it totally vanishes. Figure 1A shows that the temperature increases as ζ increases, and the penetration inside the medium decreases as ζ increases. Figure 1B shows the GL model possessing the maximum temperature at the surface with lower penetration and that CTE has the maximum penetration into the medium; it is also noted that the LS model has a weak slope near the surface.

Figure 2 contains two sub-figures, these are as follows: Figure 2A, which displays the temporal surface temperature $\theta(0, 0.0001, t)$ per q_0 for different ζ values, namely, $\zeta = 0$, $\zeta = 5 \times 10^{-4}$ and $\zeta = 8 \times 10^{-4}$ for LS theory, and Figure 1B, which describes the temporal surface temperature $\theta(0, 0.0001, t)$ per q_0 for a fixed ζ value, that is, $\zeta = 5 \times 10^{-4}$ considering the three models. The general behavior of the two sub-figures could be stated in the following statement" *The temperature increases until it achieves its maximum with a notably shift from the maximum of laser pulse; after that decreases but it will not be totally eliminated, see [30] for more explanation*". From Figure 2A, we note that the temperature achieves its peak at a longer time when ζ is small enough, which makes the peak value increase with ζ. We also note that the peak gets closer to the profile with greater ζ. At the same time, the curves preserve their behavior even after the laser turns off. In Figure 2B, we see that the LS model gets its peak at a time closer to the maximum of $\eta(t)$. In addition, this model has the greatest maximum temperature compared with other two models.

The spatial carrier density distribution N represented in Figure 3, as the previous sub-Figure 3A, outlines the carrier distribution N for $\zeta = 0$, $\zeta = 5 \times 10^{-4}$ and $\zeta = 8 \times 10^{-4}$ at time $t = 4 \times 10^{-3}$, and sub-Figure 3B describes the carrier density distribution N for a fixed ζ value, that is, $\zeta = 5 \times 10^{-4}$, considering the three models. The effect that took place by the parameter ζ can be clearly seen in Figure 3A that it is inversely proportional to the plasma. In Figure 3B, the model of LS possesses the greatest carrier density at the surface, while the GL model possesses the lower carrier density. Moreover, it is noted that penetration is approximately the same for the three models.

The spatial displacement u represented by Figure 4, as the previous sub-Figure 4A outlines the displacement distribution u for $\zeta = 0$, $\zeta = 5 \times 10^{-4}$ and $\zeta = 8 \times 10^{-4}$ at time $t = 4 \times 10^{-3}$ and sub-Figure 4B describes the displacement distributions u for a fixed ζ value, that is, $\zeta = 5 \times 10^{-4}$, considering the three models. The displacement appears in a region close to the surface and attains negative values; from Figure 4A that represents the effect of ζ, it is clearly seen that the displacement has the same value for all values of ζ at the surface and different penetration inside the medium. Figure 4B describes the case of the three mentioned models; it is noted that the GL model possesses the greatest displacement at the surface, while the CTE possesses the smallest displacement, and the penetration of the three models is slightly the same.

Figure 5 contains two sub-figures; these are as follows: Figure 5A, which displays the stress σ_{xx} per q_0 for $\zeta = 0$, $\zeta = 5 \times 10^{-4}$ and $\zeta = 8 \times 10^{-4}$ for LS theory, and Figure 5B, which describes the stress σ_{xx} per q_0 for a fixed $\zeta = 5 \times 10^{-4}$, considering the three models. In both cases, the figure contains a small sub-figure representing the stress distribution in a region close to the surface; this figure shows that the stress obeys the given boundary condition. As for Figure 5A, we see that the positive peak getting smaller as ζ increases. We note that all curves matched together on the illuminated surface until the positive peak is achieved; after that, for a larger ζ, the gradient gets steeper. We can also see that when $\zeta = 0$, the penetration takes the largest value. In Figure 5B, the curve behavior is preserved as in Figure 5A, and the positive peak of the GL model is the greatest, while that of the CTE is the smallest; moreover, the penetration of the CTE is the greatest.

Figure 6 contains two sub-figures; these are as follows: Figure 6A, which displays the stress σ_{xz} per q_0 for $\zeta = 0$, $\zeta = 5 \times 10^{-4}$ and $\zeta = 8 \times 10^{-4}$ for LS theory, and Figure 6B, which describes the stress σ_{xz} per q_0 for a fixed $\zeta = 5 \times 10^{-4}$, considering the three models. Figure 6A shows that the increment of ζ caused a delay in both negative and positive peaks. Figure 6B shows that the only model with a negative peak near to the surface is that of LS, and also, LS possesses the highest peaks in both cases (negative and positive peaks).

8 Conclusion

In this paper, we introduced a fully coupled system of equations that represents thermal, plasma, elastic, and microelongation effects, and the novel system based on three different theories of thermoelasticity. This system has been applied to 2D TE microelongated semiconducting half space whose properties are temperature-dependent, considering the volumetric absorption illumination induced by a pulsed laser. From the forgoing discussions, we can conclude that

- The obtained results are in line with the physical interpretations.
- A clear effect for the temperature-dependent properties on all variables.
- The GL and CTE models consume more energy and take longer time than the LS model to achieve their peaks.

Data availability statement

The original contributions presented in the study are included in the article/Supplementary Material; further inquiries can be directed to the corresponding author.

Author contributions

KL: conceptualization and methodology. MM: software and data curation. IT: writing—original manuscript preparation. KL: supervision. JA: visualization and investigation. AE-B: software, validation, and writing—reviewing and editing. All authors contributed to the article and approved the submitted version.

Conflict of interest

The authors declare that the research was conducted in the absence of any commercial or financial relationships that could be construed as a potential conflict of interest.

Publisher's note

All claims expressed in this article are solely those of the authors and do not necessarily represent those of their affiliated organizations, or those of the publisher, the editors, and the reviewers. Any product that may be evaluated in this article, or claim that may be made by its manufacturer, is not guaranteed or endorsed by the publisher.

References

1. Biot MA. Thermoelasticity and irreversible thermodynamics. *J Appl Phys* (1956) 27(3):240–53. doi:10.1063/1.1722351

2. Sherief H, El-Sayed AMA, Abd El-Latief AM. Fractional order theory of thermoelasticity. *Int J Sol Struct* (2010) 47(2):269–75. doi:10.1016/j.ijsolstr.2009.09.034

3. Lord HW, Shulman Y. A generalized dynamical theory of thermoelasticity. *J Mech Phys Sol* (1967) 15(5):299–309. doi:10.1016/0022-5096(67)90024-5

4. Awad E, Fayik M, El-Dhaba AR. A comparative numerical study of a semi-infinite heat conductor subject to double strip heating under non-Fourier models. *Eur Phys J Plus* (2022) 137:1303. doi:10.1140/epjp/s13360-022-03488-8

5. Fayik M, Alhazmi SE, Abdou MA, Awad E. Transient finite-speed heat transfer influence on deformation of a nanoplate with ultrafast circular ring heating. *Mathematics* (2023) 11:1099. doi:10.3390/math11051099

6. Sherief HH, Elmisiery AEM, Elhagary MA. Generalized thermoelastic problem for an infinitely long hollow cylinder for short times. *J Therm Stresses* (2004) 27(10):885–902. doi:10.1080/01495730490498331

7. Sherief HH. On uniqueness and stability in generalized thermoelasticity. *Q Appl Math* (1987) 44:773–8.

8. Henain EF, Hassan AF, Megahed F, Tayel IM. Thermo-elastic half space under illumination of a laser beam using Lord and Shulman theory. *J Therm Stresses* (2014) 37(1):51–72. doi:10.1080/01495739.2013.839431

9. Green AE, Lindsay KA. Thermoelasticity. *J Elast* (1972) 2(1):1–7. doi:10.1007/BF00045689

10. Sherief AHH. State space approach to thermoelasticity with two relaxation times. *Int J Eng Sci* (1993) 31(8):1177–89. doi:10.1016/0020-7225(93)90091-8

11. Sherief HH, Hussein EM. Fundamental solution of thermoelasticity with two relaxation times for an infinite spherically symmetric space. *J App Math Phys* (2017) 68(2):1–14. doi:10.1007/s00033-017-0794-8

12. Mahdy AMS, Lotfy K, El-Bary A, Tayel IM. Variable thermal conductivity and hyperbolic two-temperature theory during magneto-photothermal theory of semiconductor induced by laser pulses. *Eur Phys J Plus* (2021) 136:651.

13. Song YQ, Bai JT, Ren ZY. Study on the reflection of photothermal waves in a semiconducting medium under generalized thermoelastic theory. *Acta Mech* (2012) 223:1545–57. doi:10.1007/s00707-012-0677-1

14. Trodovic DM, Nikolic PM, Bojicic AI. Photoacoustic frecuency transmissin technique: Electronic deformation mechanism in semiconductors. *J Appl Phys* (1999) 85:7716. doi:10.1063/1.370576

15. Trodovic DM. Plasma, thermal and elastic waves in semeconductors. *Rev Sci Instrum* (2003) 74(1):528. doi:10.1063/1.1523133

16. Lotfy K. Effect of variable thermal conductivity during the photothermal diffusion process of semiconductor medium. *Silicon* (2019) 11:1863–73. doi:10.1007/s12633-018-0005-z

17. Lotfy K, El-Bary AA. Thomson effect in thermo-electro-magneto semiconductor medium during photothermal excitation process. In: *Waves random complex media* (2020). doi:10.1080/17455030.2020.1838665

18. Saeed AM, Lotfy K, El-Bary AA. Effect of variable thermal conductivity and magnetic field for the generated photo-thermal waves on microelongated semiconductor. *Mathematics* (2022) 10:4270. doi:10.3390/math10224270

19. Ezzat M. A novel model of fractional thermal and plasma transfer within a non-metallic plate. *Smart Struct Syst* (2021) 27(1):73–87. doi:10.12989/sss.2021.27.1.073

20. Abbas I, Hobiny A, Marin M. Photo-thermal interactions in a semi-conductor material with cylindrical cavities and variable thermal conductivity. *J Taibah Univ Sci* (2020) 14(1):1369–76. doi:10.1080/16583655.2020.1824465

21. El-Bary AA, Youssef HM. Characterization of the photothermal interaction due to ramp-type heat on a semiconducting two-dimensional solid cylinder based on the Lord–Shulman model by using double Laplace transform. *Mech Based Des Struct Mach* (2021). doi:10.1080/15397734.2020.1833740

22. Tayel IM, Lotfy K. Photothermal effects in semiconductors induced by surface absorption of a uniform laser radiation under modified Green–Lindsay theory. *Eur Phys J Plus* (2021) 136:932. doi:10.1140/epjp/s13360-021-01941-8

23. Mohammed MAY, Tayel IM. Photothermal influences in semiconductors with temperature-dependent properties generated by laser radiation using strain–temperature rate-dependent theory. *Eur Phys J Plus* (2022) 137:703. doi:10.1140/epjp/s13360-022-02910-5

24. Lomakin VA. *Theory of nonhomogeneous elastic bodies*. Moscow (1976).

25. Ezzat MA, Othman MI, El-Karamany AS. The Dependence of the Modulus of elasticity on the reference temperature in generalized thermoelasticity. *J Thermoelast* (2001) 24:1159–76.

26. Youssef HM. Dependence of modulus of elasticity and thermal conductivity on reference temperature in generalized thermoelasticity for an innite material with a spherical cavity. *Appl Math Mech* (2005) 26:470–5. doi:10.1007/BF02465386

27. Allam MN, Elsibai KA, Aboudlregal AE. Magneto-thermoelasticity for an innite body with a spherical cavity and variable properties without energy dissipation. *Int J Sol Struct.* (2010) 47:2631–8. doi:10.1016/j.ijsolstr.2010.04.021

28. Othman MIA, Tantawi RS, Eraki EEM. Effect of initial stress on a semiconductor material with temperature dependent properties under DPL model. *Microsyst Technol* (2017) 23:5587–98. doi:10.1007/s00542-017-3326-8

29. Tayel IM, Mohamed M. Surface absorption illumination in a generalized thermoelastic layer under temperature-dependent properties using MGL model. In: *Waves in random and complex media* (2021). doi:10.1080/17455030.2021.1974120

30. Tayel IM. Generalized functionally graded thermoelastic layer under the effect of volumetric absorption of laser radiation. *Mech Based Des Struct Mach* (2022) 50(10). doi:10.1080/15397734.2020.1814155

31. Tayel IM, Hassan AF. Heating a thermoelastic half space with surface absorption pulsed laser using fractional order theory of thermoelasticity. *J Theor Appl Mech* (2019) 57(2):489–500. 10.15632/jtam-pl/105469.

32. Lotfy K, Hassan W, El-Bary A, Kadry M. Response of electromagnetic and Thomson effect of semiconductor mediumdue to laser pulses and thermal memories during photothermal excitation. *Resu Phys* (2020) 16:102877. doi:10.1016/j.rinp.2019.102877

33. Khamis AK, El-Bary AA, Lotfy K, Bakali A. Photothermal excitation processes with refined multi dual phase-lags theory for semiconductor elastic medium. *Alex Eng J* (2020) 59(1):1–9. doi:10.1016/j.aej.2019.11.016

34. Alzahrani FS, Abbas IA. Photo-thermal interactions in a semiconducting media with a spherical cavity under hyperbolic two-temperature model. *Mathematics* (2020) 8(4):585. doi:10.3390/math8040585

35. Hobiny A. Effect of the hyperbolic two-temperature model without dissipation on photo-thermal interaction in a semi-conducting medium. *Results Phys* (2020) 18: 103167. doi:10.1016/j.rinp.2020.103167

36. Abbas I, Saeed T, Alhothuali M. Hyperbolic two-temperature photo-thermal interaction in a semiconductor medium with a cylindrical cavity. *Silicon* (2020) 13: 1871–8. doi:10.1007/s12633-020-00570-7

37. Shaw S, Mukhopadhyay B. Moving heat source response in a thermoelastic microelongated solid. *J Eng Phys Thermophys* (2013) 86:716–22.

38. Ailawalia P, Sachdeva SK, Pathania DS. Internal heat source in thermoelastic microelongated solid under green lindsay theory. *J Theor Appl Mech* (2016) 46:65–82. doi:10.1515/jtam-2016-0011

39. Ailawalia P, Singla A. A thermoelastic microelongated layer immersed in an infinite fluid and subjected to laser pulse heating. *Mech Mech Eng* (2019) 23:233–40. doi:10.2478/mme-2019-0031

40. Othman MIA, Atwa SY, Eraki EE, Ismail MF. A thermoelasticmicro-elongated layer under the effect of gravity in the context of the dual-phase lag model. *J Appl Math Mech* (2021) 101(12):e202100109. doi:10.1002/zamm.202100109

41. Othman MIA, Ismail MF. The gravitational field effect on a micro-elongated thermoelastic layer under the fluid load, using the lord-shulman theory and dual-phase-lag model. *Multidis Model Mater Struct* (2022) 18(5):757–71.

42. Cicco D, Nappa L. On the theory of thermomicrostretch elastic solids. *J Therm Stress* (1999) 22:565–80.

43. Eringen AC. Microcontinuum field theories. In: *Foundations and solids*, 1. New York, NY, USA: Springer (1999).

44. Eringen AC. Linear theory of micropolar elasticity. *J Math Mech* (1966) 15: 909–23.

45. Eringen AC. Theory of thermo-microstretch elastic solids. *Int J Eng Sci* (1990) 28: 1291–301.

46. Othman MIA, Jahangir A, Nadia A. Microstretch thermoelastic solid with temperature-dependent elastic properties under the influence of magnetic and gravitational field. *J Braz Soc Mech Sci Eng* (2018) 40:332. doi:10.1007/s40430-018-1204-7

47. Tzou DY. Experimental support for the lagging behavior in heat propagation. *J Thermophys Heat Transfer* (1995) 9(4):686–93. doi:10.2514/3.725

48. Tayel IM, Lotfy K, El-Bary AA, Alebraheem J, Mohammed MAY. Microelongated thermo-elastodiffusive waves of excited semiconductor material under laser pulses impact. *Mathematics* (2023) 11:1627. doi:10.3390/math11071627

Glossary

λ and μ	Lamé's constants
$\delta_n = (3\lambda + 2\mu)d_n$	Deformation potential difference
d_n	Electronic deformation coefficient
T	Absolute temperature
N	Carrier density
T_0	Reference temperature
$\gamma_1 = (3\lambda + 2\mu)\alpha_{t_1}$	Volume thermal expansion
α_{t_1}	Linear thermal expansion
σ_{ij}	Microelongation stress
P	Density
K	Thermal conductivity
C_E	Specific heat at constant strain
n_0	Equilibrium-free carrier at temperature T
D_E	Carrier diffusion coefficient
P	Density
C_E	Specific heat at constant strain
T	Photo-generated carrier lifetime
E_g	Energy gap
$e_{i,j}$	Strain tensor component
j_0	Microinertia of the microelement
$\lambda_1, \lambda_2.\alpha$	Microelongational material constants
τ_0, v_0	Thermal relaxation times
Φ	Scalar microelongational function
m_k	Microstretch component
$s = s_{ii}$	Stress tensor component